CHAPTER SEVENTEEN

Scaling biodiversity under neutrality

LUÍS BORDA-DE-ÁGUA
University of Georgia
STEPHEN P. HUBBELL
University of Georgia, Smithsonian Tropical Research Institute
FANGLIANG HE
University of Alberta

Introduction

To better understand biodiversity scaling, it may be useful to characterize the biodiversity scaling relationships that arise from the neutral perspective. This exercise will help in formulating quantitative null hypotheses for observed biodiversity scaling relationships. Here we use the term *biodiversity* to refer not only to species richness, but also to relative species abundance, and *biodiversity scaling* to refer to how patterns of biodiversity change on increasing sampling (spatial) scales. The study of biodiversity includes questions about the spatial dispersion and geographic range of species, relative species abundance, endemism, and beta diversity, the turnover of species across landscapes. A full discussion of all-taxa biodiversity scaling in the context of neutral theory is beyond the scope of the present theory because the theory currently applies only to communities of trophically similar species (a tree community, for example). It is also individual based rather than biomass based. Despite these limitations neutral theory is nevertheless a mechanistic, dynamical theory of community assembly based on fundamental demographic processes (birth, death, dispersal, speciation) – even though its postulated assembly rules are extremely simple. Under current neutral theory, speciation, ecological drift (demographic stochasticity in birth and deaths), and dispersal govern the presence or absence and the abundance of species in communities over local to global scales. Extinction is also critically important, but under neutrality, the extinction rate can be predicted once the other three processes are known. Neutral theory asserts that, to a first approximation, trophically similar species are identical (symmetric) in these vital rates on a per-capita basis. According to the theory, species develop differences in abundance due to demographic stochasticity and accidents of dispersal. Once species become differentiated in abundance, their expected fates diverge. Common species are expected to have longer life spans and to be more persistent members of local communities than rare species.

Scaling Biodiversity, ed. David Storch, Pablo A. Marquet and James H. Brown. Published by Cambridge University Press.

Since publication of the original neutral theory (Hubbell, 1997, 2001; Bell, 2000, 2001), there have been a number of significant theoretical advances, and many of the problems that were originally studied only by simulation now have analytical solutions (Volkov *et al*., 2003; Vallade and Houchmandzadeh, 2003; Houchmandzadeh & Vallade, 2003; McKane, Alonso & Solé, 2004; Etienne & Olff, 2004). One of the most significant advances has been the incorporation of symmetric density- and frequency-dependence (Volkov *et al*. 2005). Here, as we study the implications of neutrality for biodiversity scaling, we make additional improvements to the theory by incorporating more realistic models of dispersal. The original formulation (Hubbell, 2001) was constructed on the foundation of the theory of island biogeography, which only treated space implicitly in the island–mainland problem studied by MacArthur and Wilson (1967). Hubbell (2001) studied a spatially explicit model by simulation, but these studies were limited to the classical "voter model" of dispersal (e.g. Holley & Liggett, 1975; Silvertown *et al*., 1992; Durrett & Levin, 1996), in which dispersal is restricted to immediately adjacent sites in a single time step. However, there is steadily accumulating evidence that dispersal in virtually all organisms is characterized not only by frequent small-distance movements, but also by occasional very large, long-distance movements (e.g. Lewis 1997; Petit *et al*., 1997; Clark *et al*., 1998). Such long-distance movements or "jump-dispersal" events, even if they occur only relatively rarely, may have potentially large effects on species distributions and on biodiversity scaling. Thus, if one wants to understand how the mechanism of dispersal affects biodiversity on local to biogeographic spatial scales, characterizing the distribution of dispersal distances (dispersal "kernels"), including long-distance events, becomes an important objective.

Several theoretical approaches have been taken to the description of dispersal kernels (for a review see Nathan & Muller-Landau, 2000). The classical approach is to assume two-dimensional Gaussian diffusion (Nagylaki, 1974), which results in a Rayleigh distribution of radially calculated dispersal distances. This approach provides a good description of spatial dispersal when the process is relatively uniform and continuous, leading to an expansion of the borders of the spatial distribution at a constant velocity. However, it was the prevalence of jump-dispersal events in natural populations that led ecologists to search for other models of dispersal that would better capture the shape of observed dispersal kernels. These kernels generally have "fat tails" relative to the Gaussian, that is, higher probability of long-distance dispersal and therefore more probability in the tails of the distribution. One such distribution is the 2Dt distribution, which has recently been fit to a large number of dispersal kernels of tree species (Clark *et al*., 1999; Muller-Landau *et al*., 2004) and used as a model for dispersal in theoretical and simulation work (Chave & Leigh, 2002; Chave, Muller-Landau & Levin, 2002).

A class of probability density functions that have not yet been widely used in ecology (Kot, Lewis & Van den Driessche, 1996; Halley & Iwasa, 1998), but that

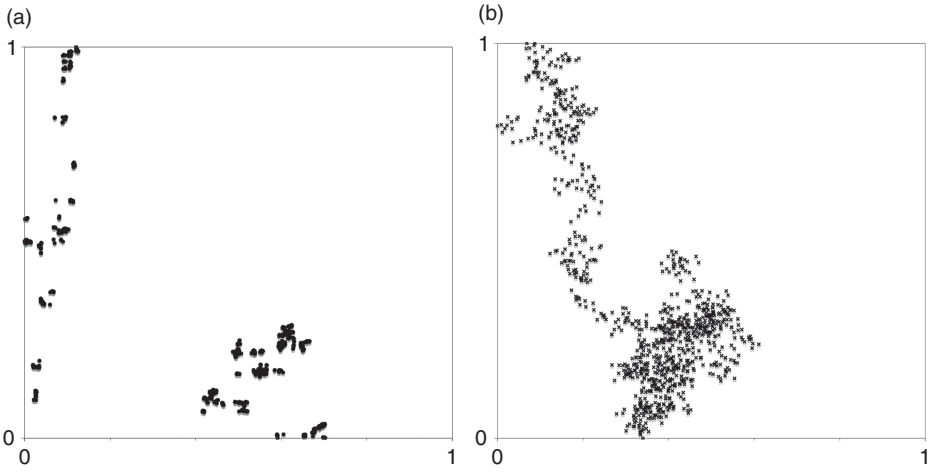

Figure 17.1 (a) Example of Lévy flights obtained with a Cauchy distribution, and (b) a typical random walk obtained with a Gaussian distribution. Lévy flights are random walks where the position of the next point is obtained by adding to the position of the previous point distances along the *x* and *y* axes sampled from Lévy stable distributions. The Gaussian is a special case of the Lévy stable distributions. Because it does not have fat tails it does not give origin to a series of well-identified clusters. In both cases we used 1000 points. The scales are arbitrary.

seem highly appropriate for describing dispersal, are the probability density functions known as Lévy stable distributions (Weiss, 1994; West & Deering, 1994; Mandelbrot, 1997; Mantegna & Stanley, 2000). Although the Gaussian (normal) distribution is a member of this class, it is a special and unusual case in that it has defined moments (e.g. mean, variance, etc.). Despite the fact that they are true probability density functions whose integrals are equal to unity, most Lévy stable distributions do not have defined moments. When used to describe dispersal, the "fat tails" of Lévy stable distributions increase the probability of occasional long-distance dispersal events, resulting in a pattern of movement unlike Brownian diffusion which tends to show the steady advance of a "front". Instead, one obtains dispersal patterns aptly termed "Lévy flights", characterized by sequences of mostly local movements, terminated by occasional long jumps to the location of a new sequence of local movements. Figure 17.1 is an example, which might represent the path taken by a series of sequential parent–offspring pairs, for the simplified case of only a single offspring produced in each time step.

An important conclusion of this work is that the population-level dispersion patterns produced by many individuals simultaneously pursuing independent Lévy flights of multiple offspring produce patterns that are characterized by multifractals. By using multifractal methods, our main purpose is to show that

a multifractal pattern is a common occurrence in the spatial distribution of tropical tree species. If observed patterns are multifractal, then the onus is on theoretical models to generate them, and the point distributions obtained with our neutral simulations do show patterns that are well described by multifractals.

This chapter is about biodiversity scaling under neutrality. However, because we are introducing more realistic Lévy stable distributions for dispersal into the theory, and because of the novelty of these distributions and of multifractals in ecology, we first discuss the patterns of dispersion that arise in single species populations under neutral dynamics with non-Gaussian, Lévy stable dispersal. Using a spatially explicit model, we show that these single species patterns are multifractal, and we describe how to analyze spatial data using multifractal methods (a more detailed account on multifractals is given in the Appendix). We then show that the patterns produced under neutrality are very similar to the multifractality observed in the spatial distribution of individual tropical tree species on Barro Colorado Island (BCI), Panama. Finally, we return to our primary question, and consider how changing the parameters of the Lévy stable dispersal function affects biodiversity scaling under neutrality. In this chapter, we only consider symmetric neutrality, such that all species exhibit the average community dispersal kernel. Elsewhere we relax this assumption and allow species to have different Lévy stable dispersal kernels. We now describe the spatially explicit model of the community used in our studies.

The model

Modeling dispersal with Lévy stable distributions

Here we consider mainly seed dispersal by terrestrial plants, but our conclusions also apply to all species that exhibit occasional long-distance "jump" dispersal events. Empirically obtained seed dispersal distributions are often convex near the source plant and have long tails (Clark *et al*., 1999; Jones *et al*., 2005) that are too "fat" relative to the standard Gaussian distribution. Therefore, we seek different distribution functions that can accommodate the observed shapes both near and far from the source (Clark *et al*., 1999). Lévy stable distributions have been rarely used in ecology but they have a venerable history in the study of fractals (e.g. Mandelbrot, 1977, 1997; West & Deering, 1994), and Gnedenko and Kolmogorov (1954) predicted the wider application of Lévy stable distributions: "All these distribution laws, called stable, ... deserve the most serious attention. It is probable that the scope of applied problems in which they play an essential role will become in due course rather wide." As mentioned, the Gaussian distribution is different from other Lévy stable distributions in two regards. First, the Gaussian distribution has moments of all orders, while, in general, Lévy stable distributions have only one moment (mean) or no moments at all. Second, the tails of the Gaussian distribution are not well described by power laws, unlike the tails of other Lévy stable distributions. From a theoretical

point of view, Lévy stable distributions result from the sum of independent, identically distributed (i.i.d.) random variables and arise from a more general form of the central limit theorem. According to the central limit theorem, the sum of i.i.d. random variables with *finite variance* converges to the Gaussian distribution. However, for distributions without finite variance (or mean), such as the Cauchy distribution, the familiar central limit theorem does not apply. It is for these other distributions that the other Lévy stable distributions are the limiting sum.

Except for a few cases, such as the Gaussian and the Cauchy, the analytical expression of the probability density function of the Lévy stable distributions is not available, but the form of their characteristic function is. For one-dimensional distributions centered at the origin and symmetrical, the characteristic function, $F(q)$, is

$$F(q) = \exp(-c\,|\,q\,|^{\alpha}), \tag{17.1}$$

where c is called the scale parameter and α the characteristic exponent. The parameter α is bounded as $0 < \alpha \leq 2$. When $\alpha = 1$ we obtain the Cauchy distribution, and when $\alpha = 2$ the Gaussian distribution. Except for $\alpha = 2$, Lévy stable distributions only have moments of order lower than α. Hence, distributions with $1 < \alpha < 2$ only have mean, and distributions with $\alpha \leq 1$ do not have moments of any order.

Although in general the form of the probability density functions is not known, it can be shown (e.g. West & Deering, 1994) that, except for the Gaussian, the tail of the probability density functions decays as a power law:

$$f(|\,x\,|) \sim |\,x\,|^{-(1+\alpha)}. \tag{17.2}$$

Figure 17.2 illustrates the probability density functions of some Lévy stable distributions for several values of α and c. The generation of Lévy stable random variables can be done easily with the algorithm suggested by Chambers, Mallows and Stuck (1976). For information on Lévy stable distributions, in addition to the references already cited, we recommend Mantegna and Stanley (2000) and Weiss (1994).

The computer model

Our model took space explicitly into account and consisted of a hexagonal lattice with 1024 by 1024 sites, where every site is occupied with a single individual of an arbitrary species. Following common practice in the study of spatially explicit models (e.g. Chave *et al.*, 2002), we used periodic boundary conditions. However, we also checked our results with a model without periodic boundary conditions, but the results were qualitatively indistinguishable. We initialized the system by sampling individuals from a pool of 100 species in which all the species had the same probability of being chosen, or were drawn

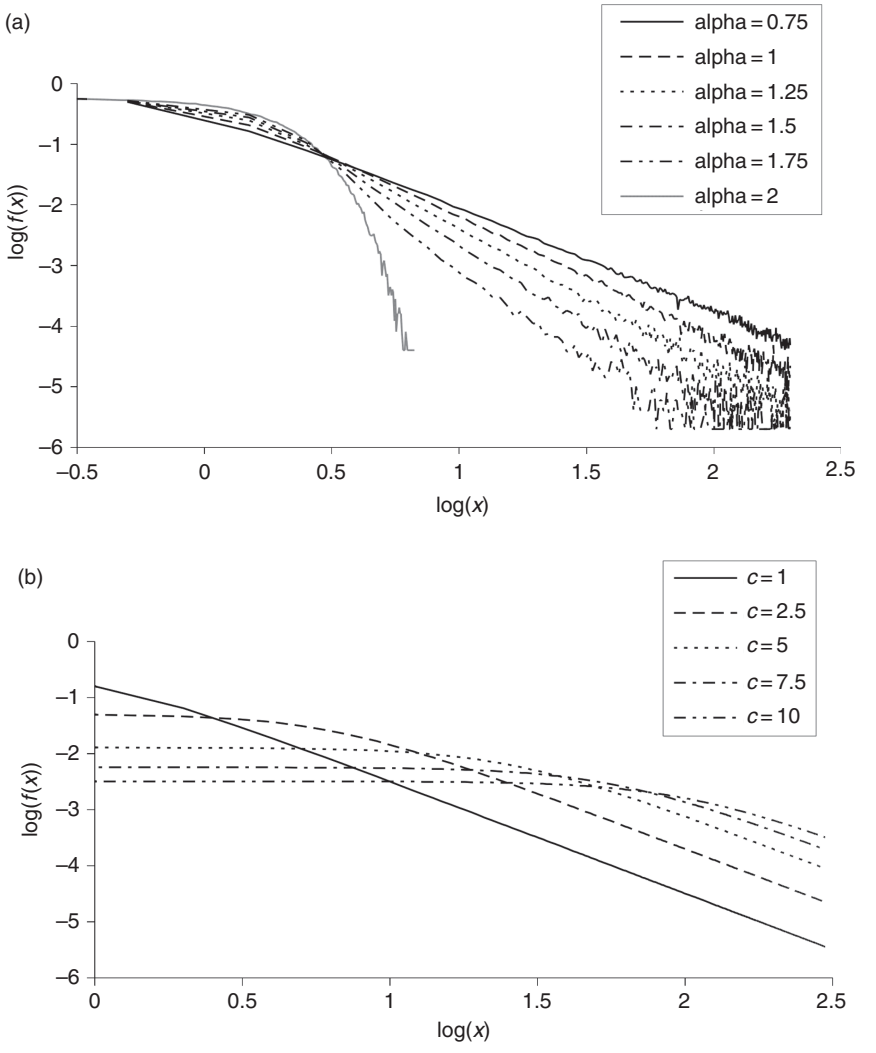

Figure 17.2 Examples of Lévy stable distributions plotted in log-log scales. In plot (a), $c = 1$ and $\alpha = 0.75$, 1.0, 1.25, 1.5, 1,75, 2.0, and in plot (b), $\alpha = 1.0$ (Cauchy distribution) and $c = 1$, 2.5, 5, 7.5, 10. Except for $\alpha = 2.0$ (Gaussian distribution) in plot (a), the tails are approximately straight lines; the slopes are equal to $-(1 + \alpha)$.

from the relative abundance distribution expected under neutrality given the size of the community and the speciation rate (Hubbell, 2001). In each iteration we removed a percentage of the individuals (deaths), and we refilled each vacant site with a new individual (birth). This new individual might be an entirely new species (speciation), with probability υ, or an individual of a species already present in the community, with probability $1 - \upsilon$. In our studies we varied the speciation rate from 10^{-7} to 10^{-4}. When the replacement was from a species

already present in the community, we chose the species by an inverse dispersal method, as follows. Centered in the site to be replaced, we randomly chose distances from a Lévy stable distribution along the x and y axes in positive or negative directions, and these distances determined the maternal site and therefore the species of the new individual. We performed two kinds of simulations, but the results were qualitatively similar. In one case, we preserved information on the lattice prior to imposing mortality so that there was always an individual present in the maternal site. In the second case, we choose the identity of the new individual only among the individuals that survived mortality. In this case, the selected maternal site may be vacant. When this happened, we repeated the search until we found an occupied site. Most of our simulations employed the first method, which was much faster to run. We ran each simulation until a well-established equilibrium was reached, meaning that after a transient the simulation has evolved to a regime where we observed no trend in the evolution of the number of species, and species–area curves and species-abundance distributions obtained at different time steps were qualitatively similar.

Chave *et al.* (2002) used a very similar model to ours. A few differences from our model to Chave *et al.* (2002) are: we used a hexagonal lattice and they used a square lattice, we used Lévy stable distributions and they used the 2Dt distribution, we did not allow for vacant sites (in the spirit of the zero-sum game as in Hubbell, 2001) and they allowed for vacant sites.

Multifractal analysis of spatial dispersion of single species populations

In this section we first analyze the spatial distribution of model species obtained with different dispersal kernels under neutrality, and we use multifractals to describe these spatial distributions. We then show, using multifractals, that similar patterns are also observed in many of the tree species in the 50 ha plot of tropical forest on Barro Colorado Island (BCI), Panama, established in 1980 (Hubbell & Foster, 1983).

Figure 17.3 shows several distributions obtained with different dispersal kernels ($c = 10$ and $\alpha = 1.0$, 1.5, and 2.0). It is obvious from visual inspection that the degree of clustering depends on the dispersal kernel used. When dispersal distances decrease, which corresponds to an increase in the parameter α of the Lévy stable distributions, the spatial dispersion patterns become more clumped. On first inspection these results might seem to contradict our previous discussion on the spatial distributions generated by Lévy flights (Fig. 17.1). However, these point distributions are being generated by a process that is different from that of a single Lévy flight. First, in the simulations, each "parent" point may give rise to more than one "offspring" point; that is, a point can start multiple new "paths". Second, there is superimposed mortality, which removes some of the points from the landscape. Third, we are using periodic boundary

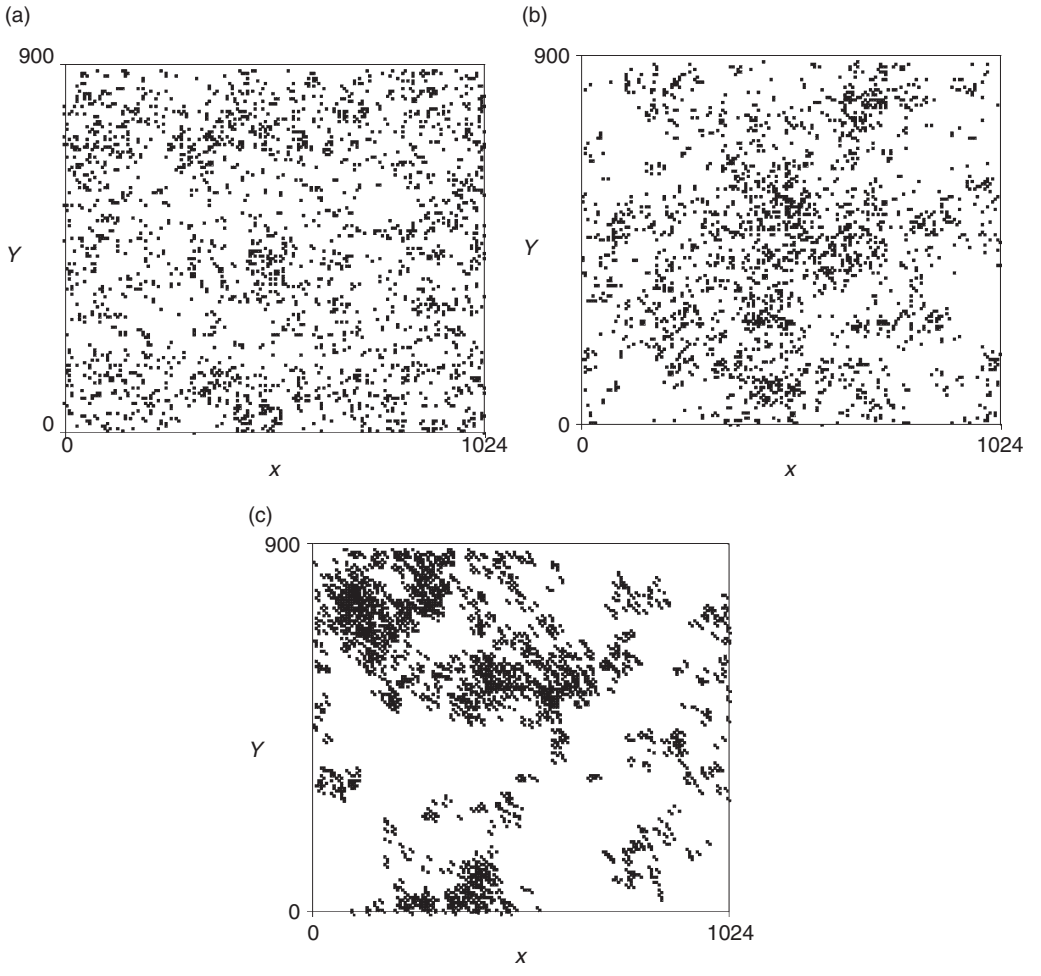

Figure 17.3 Example of spatial distributions generated with simulations using a neutral model. Plot (a) was obtained with $\alpha = 1.0$ (Cauchy distribution), plot (b) with $\alpha = 1.5$, and plot (c) with $\alpha = 2.0$ (Gaussian distribution). Notice that an increase in the value of α leads to more clumped distributions.

conditions, which means that points that leave the plot from one side re-enter from the opposite side of the plot; hence, points are closer together than one would expect from a Lévy flight. This periodic boundary effect is equivalent to assuming immigration from adjacent areas of the simulated forest. Since the resulting single-species dispersion patterns are well described by multifractals, we now turn to a description of multifractal methods.

Definition of multifractals

Most objects including point distributions that exhibit fractality are, in fact, multifractal, so multifractal methods provide a more accurate description of

such objects. The difference between fractals and multifractals lies in the detail of information used about the pattern that one is describing. In describing point distributions using fractals alone, we only use information about presence or absence. In describing point distributions using multifractals, we also use information about relative abundance. Adapting an example from Evertsz and Mandelbrot (1992), imagine a large geographical area, say, South America. If South America is divided into two regions of equal area, one region is likely to have a larger forested area than the other. If one of these regions is again subdivided into two equal areas, one of these subareas may have a larger forested area than the other. As the subdivision continues, it is likely that each of the subdivided regions will have a different proportion of forested area. Forest area is thus an "irregular" measure at all spatial scales. Now let this irregularity be self-similar, such that each time we make a subdivision, the proportions of forested area in the two halves remain the same, say p_1 and p_2. This means that in the next division of these areas, we obtain fractions p_1p_1, p_1p_2, p_2p_1, and p_2p_2. In this case, we say that the irregularity is the same ("self-similar") at all scales, and the process by which it was obtained is called a multiplicative cascade. At each scale of the construction of the multifractal we can construct histograms of values associated with the fractions in the subdivisions. The objective of the multifractal analysis is to describe the scaling properties of these histograms, which is achieved after appropriate renormalizations (Evertsz & Mandelbrot, 1992). However, dealing directly with the histograms is a very inefficient process, and, instead, we deal with the moments of the distributions and observe the scaling properties of the moments. In the next section we give a brief account of the method used in this work and give more detailed information in the Appendix.

Estimating multifractal spectra

Whereas a fractal is described by a single number, the fractal dimension, a multifractal requires a spectrum of "dimensions"; notice the quotation marks because not all values of the spectrum can be properly interpreted as dimensions. For the purposes of this work we use the spectrum of generalized dimensions, D_q (see Everstz & Mandelbrot, 1992, for another type of multifractal spectrum). There are several methods to estimate the multifractal spectrum but not all are equally adequate for calculating all parts of the spectrum. For reasons explained in the Appendix, we use the fixed-mass method.

The fixed-mass method is based on the following relationship, valid for multifractals,

$$\langle R_i(m)^{-\tau_q}\rangle^{1/\tau_q} \sim m^{-1/D_q}, \tag{17.3}$$

where $\langle\ \rangle$ stands for average over all points, R for radius, m for the number of points in the vicinity of a given point i, and τ_q is a real number related to D_q through the relationship $\tau_q = (q-1)D_q$, and q is also a real number ranging

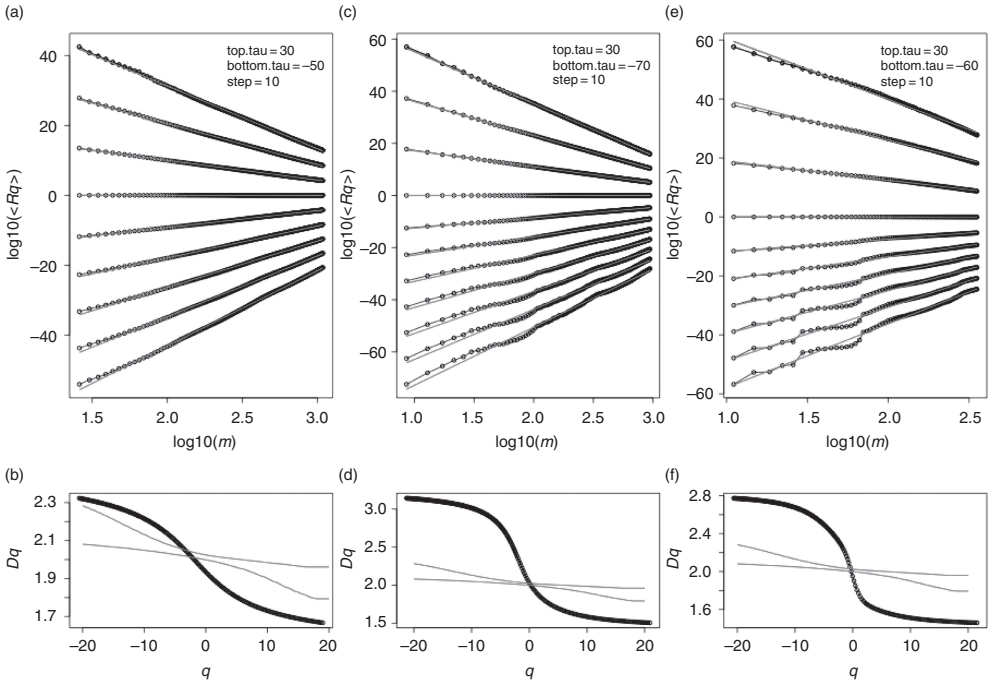

Figure 17.4 Plot (a) shows the curves of $\log_{10}(\langle R_q \rangle) = \log_{10}(\langle R_i(m)^{-\tau_q} \rangle^{1/\tau_q})$ versus $\log_{10}(m)$ for the point distribution shown in Fig. 17.3(a) and obtained with $\alpha = 1.0$. From this plot we estimate the slope from which we obtain q, used for the construction of plot (b), showing the spectrum of generalized dimensions D_q. Notice that D_q is a monotonically decreasing function of q. Plots (c) and (d), and (e) and (f) are the same for the distributions of Fig. 17.3(b) and Fig. 17.3(c), respectively. The red solid lines in plots (b), (d) and (f) consist of the largest and the smallest D_q values obtained from 200 Poisson processes with the same number of points as the original distribution. (For color version see Plate 11.)

from $-\infty$ to $+\infty$. As we will see below, q plays an important role in the characterization of a multifractal. The main idea in the fixed-mass method is to determine the minimum radius from a point i, R_i, that contains m points, $R_i(m)$. The method consists of calculating $R_i(m)$ for all points in the plot and, then, the average $\langle R_i(m)^{-\tau_q} \rangle$ for several values of τ_q. This process is repeated for several values of m, and, in order to assess and characterize the multifractality, we plot $\log\left(\langle R_i(m)^{-\tau_q} \rangle^{1/\tau_q}\right)$ as function of $\log(m)$; see Fig. 17.4(a, c, e) and Fig. 17.6(a, c, e). For a multifractal we should observe a linear relationship, or a linear relationship with oscillations superimposed (see Box 17.1). From these curves we estimate the slope, which corresponds to $-1/D_q$. We then use the relationship $\tau_q = (q-1)D_q$ to calculate q and, finally, we draw D_q as a function of q, which is the spectrum of generalized dimensions. The D_q spectrum is a monotonically decreasing function, sigmoid in shape; Fig. 17.4(b, d, f) and Fig. 17.6(b, d, f) show several D_q spectra.

Box 17.1 Power laws, oscillations and self-similarity

Power laws, such as $y = ax^b$, are not the only family of curves that are self-similar, although the estimation of fractal dimensions is usually performed by trying to fit a straight line in a log-log plot. A more general form that is still self-similar is

$$y = ax^b f\left(\frac{\log(x)}{\log(c)}\right), \tag{17.4}$$

where a, b, and c are constants and $f(z)$ is a function such as $f(z) = f(1+z)$ (Liebovitch, 1998). When plotted in a log-log plot, the curve obtained with this function is a straight line on which periodic oscillations are superimposed. Hence, whenever we see such a pattern we consider it evidence of self-similarity. However, the presence of these oscillations makes the estimation of the slope associated with the power law more difficult, and may in some cases cause one to erroneously reject the hypothesis of self-similarity even when the pattern may truly be self-similar (Badii & Polity, 1984; Meneveau & Sreenivasan, 1989).

Changing q, or τ_q, is somehow analogous to obtaining the moments of a probability density function. As explained in more detail in the Appendix, by choosing different q values we select regions of the plane with different point densities. The part of the D_q spectrum associated with positive values of q gives information on dense regions of the point distribution, and the part associated with negative q values gives information on sparse regions of the point distribution. In the case of a perfect fractal, all generalized "dimensions" are equal and the spectrum is a horizontal line parallel to the q-axis, and in the special case of a Poisson process in a plane $D_q = 2$. Deviances from a horizontal line are a measure of the heterogeneity of the point spatial distribution (see next section for examples on the estimation of multifractal spectra and the Appendix for more detailed information).

Some values of q lead to well-known fractal dimensions: $q = 0$ corresponds to the box-counting dimension, and $q = 2$ corresponds to the correlation dimension. In the following sections we will pay special attention to these two fractal dimensions for two reasons. First, because we want to show that the box-counting dimension is sometimes misleading, since we obtain a value close to 2 although the distribution is not that of a Poisson process, and, second, because D_2 has a straightforward interpretation in terms of the degree of clustering: when D_2 is equal to the topological dimension, 2 in the case of a plane, the points are distributed according to a Poisson process, often called complete spatial randomness, and when D_2 is smaller than the topological dimension the points are clustered, and the degree of clustering increases as D_2 decreases.

To see this, think of a Poisson process and of a clustered distribution with the same number of points in an area of equal size and shape. For the Poisson distribution, the number of points increases as R^2 increases. For a clustered distribution when R is small, the number of points increases faster than predicted by the Poisson distribution precisely because the points are clumped. However, after a certain value of R, voids start to dominate the clustered distribution, and thereafter the number of points increases more slowly than predicted by the Poisson distribution. Since for a fractal the number of points increases as R^{D_2}, then $D_2 < 2$.

Spatial distributions of model species under neutrality

We now apply multifractals methods to analyze the spatial distributions of model species under neutrality with Lévy stable dispersal, and for a representative set of common tree species in BCI. In order to establish multifractality we required that a scaling region (i.e. $\log(\langle R_i(m)^{-\tau_q}\rangle^{1/\tau_q})$ versus $\log(m)$) be observed for at least one order of magnitude, and we required that the D_q spectrum is a monotonically decreasing function.

We first analyze the distributions of species obtained by simulations under neutrality. As previously discussed, Fig. 17.3 shows that point distributions obtained with larger values of α are more clustered than those obtained with smaller α. We now show how these characteristics are reflected in the multifractal spectrum and the steps that one always goes through in multifractal analysis. Consider the point process in Fig. 17.3(a). The estimation of the multifractal spectrum starts with the calculation of the $\log(\langle R_i(m)^{-\tau_q}\rangle^{1/\tau_q})$ curves, each obtained for a fixed value of τ_q (Fig. 17.4a). In order to avoid cluttering the figure, we show only curves for a few values of τ_q, but we used more values to obtain the final estimation of the D_q spectrum. We chose a large range of τ values to accommodate q values in the range –20 to 20, with special interest in values of q close to 0 and 2. The next step is to assess if the curves of $\log(\langle R_i(m)^{-\tau_q}\rangle^{1/\tau_q})$ are well fit by straight lines. This is clearly true for the distribution in Fig. 17.4(a). Note that the linear relationships extend for more than one order of magnitude, $26 \leq m \leq 1082$. In fact, we could not identify an upper cutoff, so we speculate that the scaling region would be further extended if a larger data set had been available. We now estimate the slopes of the lines in Fig. 17.4(a), which are equal to $-1/D_q$, determine q using $q = 1 + \tau_q/D_q$, and plot the multifractal spectrum (Fig. 17.4b). This figure shows that the D_q spectrum is a monotonically decreasing function of q, as expected for a multifractal distribution. We estimate D_0 and D_2 from $\tau = -2$ and $\tau = 2$, leading, respectively, to $q = -0.03$ ($\approx$0.0) and $q = 2.07$ ($\approx$2.0), and from $D_q = \tau_q/(q-1)$, $D_0 = 2.004$, and $D_2 = 1.87$. The width of the spectrum, which is a measure of the difference between the scaling properties of the regions with higher and lower density of points, is $\Delta D_{-20-20} = D_{-20} - D_{20} = 0.656$ (we chose D_{-20} and D_{20} because it corresponds to the limits of the q values used

to describe the multifractal spectrum). D_0 is slightly larger than the maximum expected, 2. This is most likely a small error due to the fitting procedure and because we used a q value slightly smaller than 0, and since D_q is a monotonically decreasing function, this may lead to the value of D_0 being slightly larger than 2, when, in fact, its true value is 2.

Although ideally a Poisson process has $D_q = 2$ for all q, it is likely that for a finite collection of points this is not the case. In order to rule out the possibility that the observed D_q spectrum is that of a Poisson process, we generated 200 Poisson processes and obtained the envelopes consisting of the largest and the smallest D_q values, shown in Fig. 17.4(b) in red solid lines. Note that the spectrum of the distribution obtained under neutrality only falls within the two envelopes of the Poisson processes in the vicinity of D_0, but that for most of the region in which $q < 0$ it lies above the envelopes of the Poisson processes and for most $q > 0$, it is below. Thus we can reject the hypothesis that the distribution of the model population under neutrality with Lévy stable dispersal is a Poisson process.

For the point distribution in Fig. 17.3(b), obtained with $\alpha = 1.5$, we estimate $D_0 = 2.03$, $D_2 = 1.84$, and $\Delta D_{-20-20} = 1.64$ (Fig. 17.4c, d, colour plate), and for the distribution in Fig. 17.3(c), obtained with $\alpha = 2.0$, we estimate $D_0 = 1.95$, $D_2 = 1.69$, $\Delta D_{-20-20} = 1.31$ (Fig. 17.4c, f). We also plotted the envelopes of the spectra of 200 Poisson processes with the same number of points as the original distributions, and in both cases we observe that, except for q close to 0, the spectrum is once again clearly outside the boundaries of the envelopes. Note that if we had reduced our analysis to D_0 (i.e. box counting), we would have concluded erroneously that the distribution was that of a Poisson process. Relative to the distribution of points obtained with $\alpha = 1.0$, we observe that D_2 decreases when α increases, in agreement with our previous finding that an increase in α leads to more clustered distributions.

Single-species distributions of BCI tree species

We now turn to the analysis of the spatial distributions of common tree species in the BCI plot. For this study, we used data from the 1995 census. The 1995 census contains 300 species and 229 072 individuals. There are 75 species in the 1995 census that have more than 500 individuals. We restricted the analysis to these common species in order to have large scaling regions for the fixed-mass method. Applying our criteria for multifractality, we conclude that a multifractal model is an excellent representation for 67 (90%) of these species. We expect that this fraction will increase when data from larger areas become available. It is not possible to present the multifractal spectra here for all the species we analyzed, so we present the multifractal spectra for species that are representative of the several patterns we found. The representative species are: *Guarea guidonia* (Meliaceae) (Fig. 17.5a), *Annona acuminata* (Annonaceae) (Fig. 17.5b), and *Rinorea sylvatica* (Violaceae) (Fig. 17.5c). We summarize the

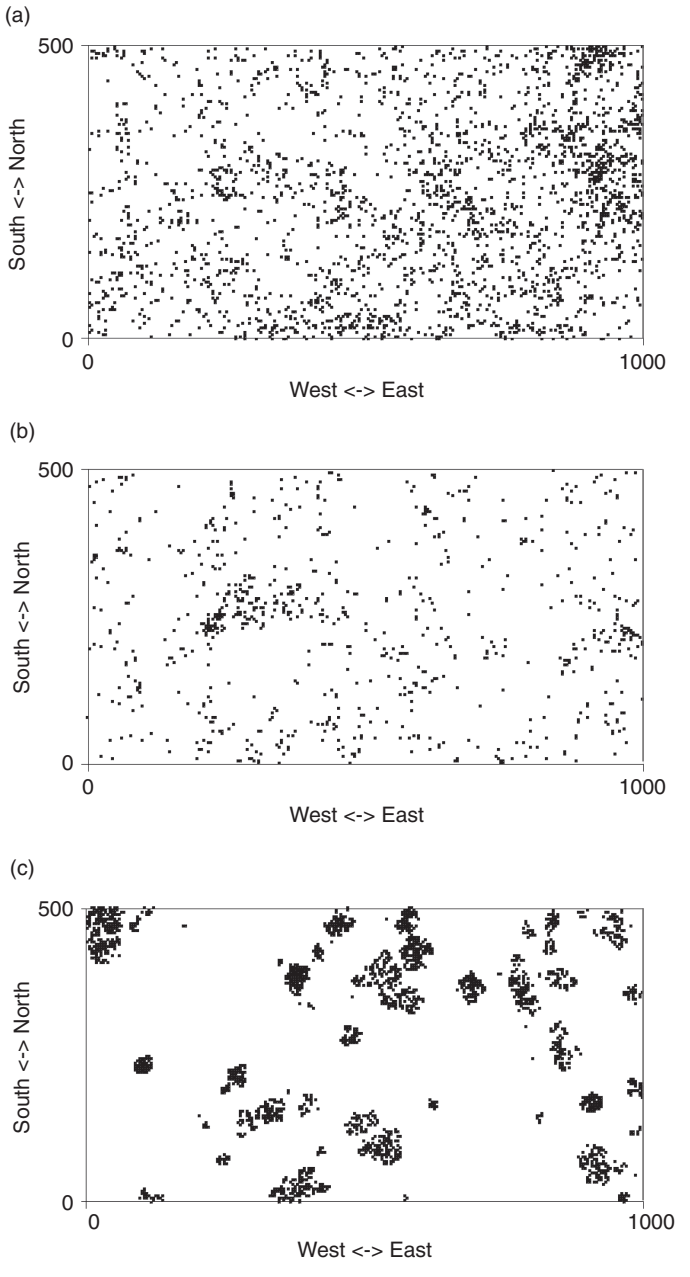

Figure 17.5 Spatial distributions of (a) *Guarea guidonia*, (b) *Annona acuminata*, and (c) *Rinorea sylvatica*.

results in terms of D_0, D_2 and the difference ΔD_{-20-20}. None of the species has a spatial distribution following a Poisson process.

The spectrum of *Guarea guidonia* (Fig. 17.6b), resembles those obtained from the neutral model species with $\alpha = 1$, but note that the width of the spectrum for *Guarea guidonia* is slightly larger, $\Delta D_{-20-20} = 0.964$, indicating a more

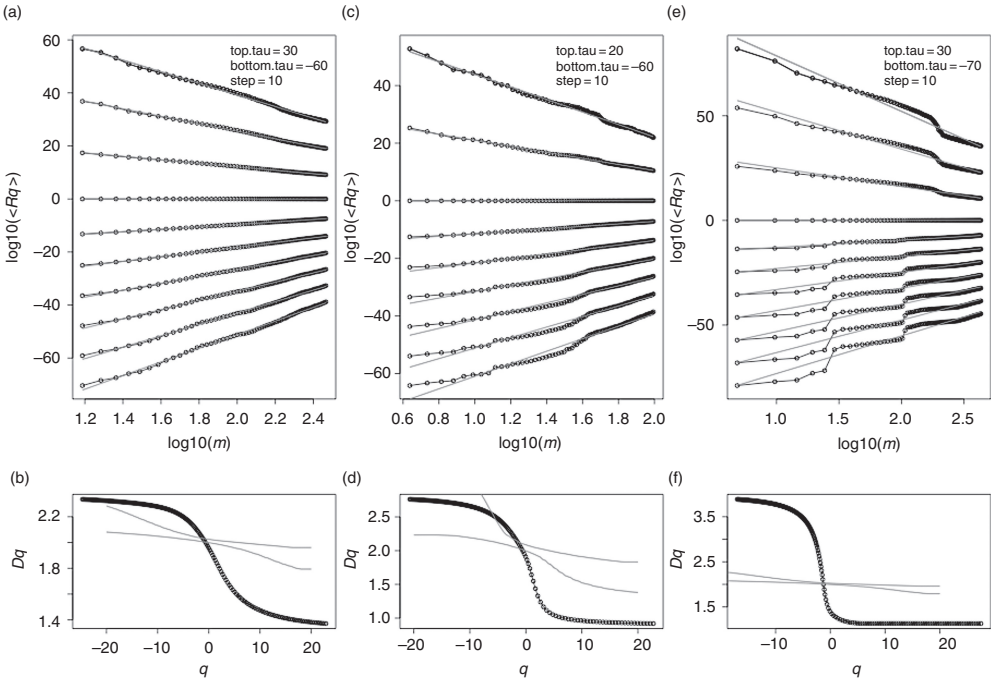

Figure 17.6 Plot (a) shows the curves of $\log_{10}(\langle R_q \rangle) = \log_{10}(\langle R_i(m)^{-\tau_q} \rangle^{1/\tau_q})$ versus $\log_{10}(m)$, and plot (b) the spectrum of generalized dimensions for the spatial distribution of *Guarea guidonia* (Fig. 17.5a), and plots (c) and (d), and (e) and (f) are the same for *Annona acuminata* (Fig. 17.5b) and *Rinorea sylvatica* (Fig. 17.5c), respectively. The red lines in plots (b), (d) and (f) consist of the largest and the smallest D_q values obtained from 200 Poisson processes with the same number of points as the original distribution. (For color version see Plate 12.)

heterogeneous distribution. The spectrum of *Annona acuminata* (Fig. 17.6d) is interesting because for negative q values, i.e. sparse regions, the spectrum is undistinguishable from a Poisson process. This conclusion follows from the fact that for negative q values, the spectrum lies completely within the envelopes of the simulated Poisson process. However, for positive q, i.e. abundant regions, it clearly lies outside the envelopes of the random simulations, and we conclude that the distribution is not that of a Poisson process. *Rinorea sylvatica* is especially intriguing because of its highly clumped distribution (see Fig. 17.5c). As expected, its multifractal spectrum (Fig. 17.6e, f), exhibits a large width ($\Delta D_{-20,-20} = 2.75$). Note the oscillations in the plot of $\log(\langle R_i(m)^{-\tau_q} \rangle^{1/\tau_q})$ as a function of $\log(m)$, and that these oscillations exhibit some periodicity. According to our discussion in Box 17.1 of a more general form of self-similarity, these oscillations do not indicate an absence of self-similarity. Such oscillations often arise in cases like *Rinorea* in which there are distinct cluster sizes.

The histograms of D_0, D_2, and $\Delta D_{-20\ -20}$ for the 67 BCI tree species with multifractal distributions are shown in Fig. 17.7. Most values of D_0 are concentrated around 2, and the reasons for occasional values slightly above 2, the theoretical maximum, have already been discussed. The species with the smallest value of D_0 was *Rinorea sylvatica*. This result is not surprising given that *Rinorea sylvatica* has a highly clustered spatial distribution. As expected, the histogram of D_2 (Fig. 17.7b) exhibits values smaller than those of D_0. D_2 values are around 1.8, although there are seven species with $D_2 < 1.4$. The species with the highest D_2 is *Desmopsis panamensis* ($D_2 = 1.95$), and the one with the smallest is *Croton billbergianus*, $D_2 = 1.15$. Other species with small D_2 values are *Palicourea guianensis*, $D_2 = 1.17$, and *Rinorea sylvatica*, $D_2 = 1.22$. All species with small D_2 values exhibit very clustered spatial distributions, as expected. Interestingly, two of the species with low D_2, *Rinorea sylvatica* and *Croton billbergianus*, have a dispersal mechanism consisting of explosive seed capsules, which almost always results in very local dispersal distances. The probability of observing 2, 3 or 4 species with explosive capsules in a sample of 7 species is 0.05 (hypergeometric sampling), indicating that a relationship exists between dispersal modes and spatial patterns. This result suggests that it would be profitable to explore further what correlations exist between the fractal dimensions of plant populations and their mechanism or mode of dispersal. We also analyzed the relationship between regeneration guilds (9 gap species versus 58 nongap species) and found that among the 7 species with $D_2 < 1.4$, 3 were gap species, which was also significant ($P = 0.046$). Also of interest is the relationship between the average D_2 of the gap species, $\overline{D_2} = 1.54$, and nongap species, $\overline{D_2} = 1.77$. A randomization test (Manly, 1997) showed that the average D_2 of the gap species is significantly smaller (one-tail test) from the average D_2 of the nongap species ($P = 0.002$).

Species with highly clustered distributions show the largest differences between the most dense and most sparse regions. For this reason, it is not unexpected that two highly aggregated gap species exhibit the largest ΔD values: *Palicourea guianensis* has the largest $\Delta D_{-20\,-20} = 4.34$, followed by *Croton billbergianus*, $\Delta D_{-20\,-20} = 3.85$. The species with the smallest $\Delta D_{-20\,-20} = 0.708$ is *Sorocea affinis*, whose spatial distribution does not exhibit any obvious clusters. Most values of $\Delta D_{-20\,-20}$ occur between 0.8 and 2.2.

Species–area relationships under neutrality

We showed in the previous sections that a neutral model with Lévy stable dispersal can lead to species distributions that are well described by multifractals. We have also shown that short distance dispersal (larger α) leads to spatial distributions that are more aggregated than those obtained with longer distance dispersal (smaller α).

The question for this section is what influence does long- versus short-distance dispersal have on the shape of species–area curves? Chave, *et al.* (2002)

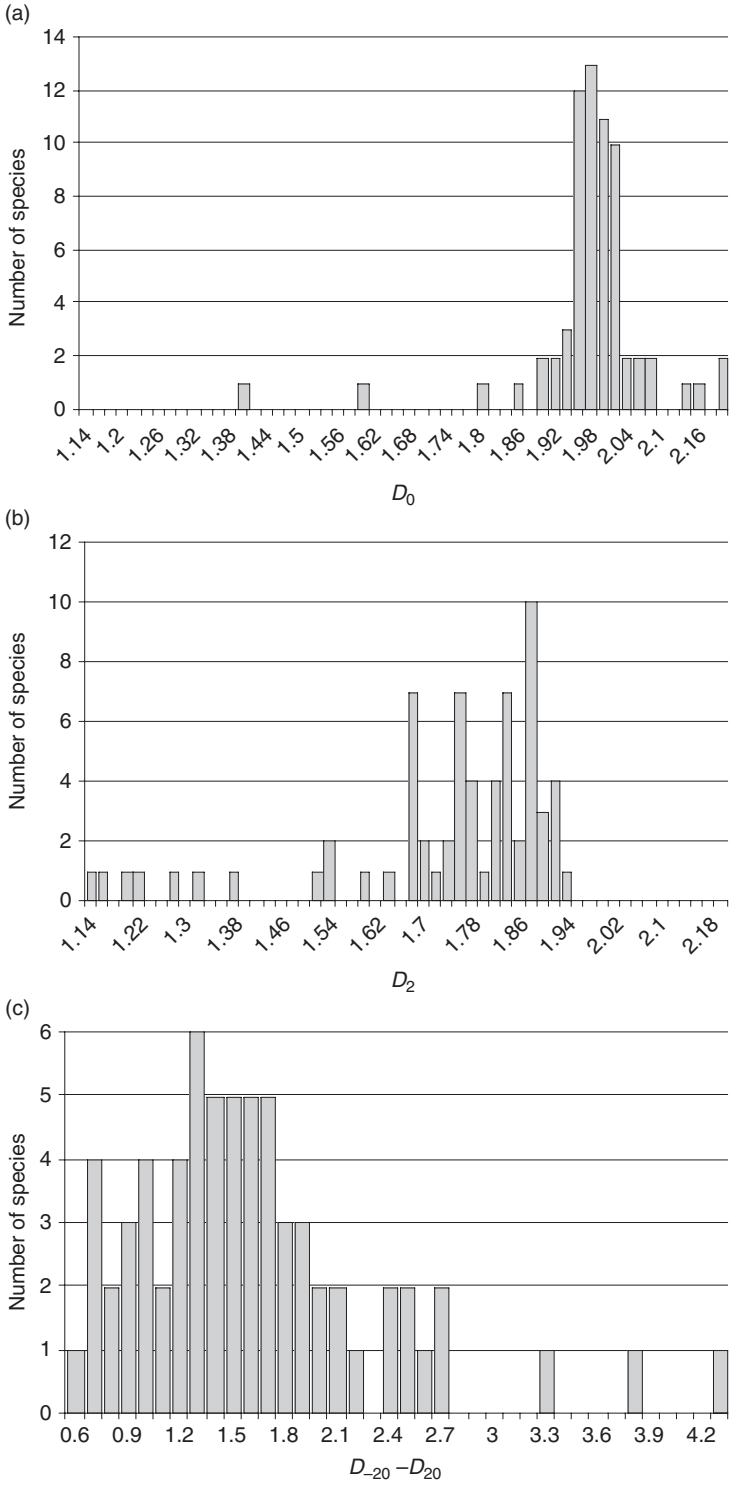

Figure 17.7 (a) Histograms of the box-counting dimension (D_0), (b) the correlation dimension (D_2), and (c) the width of the D_q spectrum (ΔD_{-20-20}) for the 67 species in the 50 ha BCI plot. Only those species with more than 500 individuals and with spatial distributions well characterized by a multifractal model were included in the analysis.

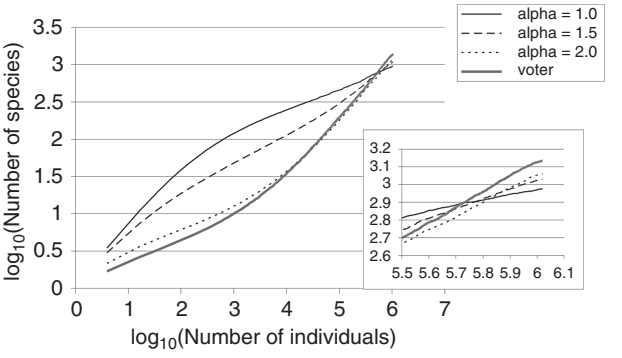

Figure 17.8 Log of the number of species as a function of the log of the number of contiguous individuals (equivalent to area) obtained with simulations using $\alpha = 1.0$, 1.5, 2.0 and the voter's model. The inset plot is an enlargement of the curves for the largest numbers of individuals.

also addressed this question and because of the similarities of our models the results are qualitatively the same. Here we model long-distance dispersal by varying the characteristic exponent, α, of the Lévy stable distribution used to model the dispersal kernel. The dispersal kernel is also affected by the scale parameter c, which determines the width of the hump at the source in the dispersal kernel, but because we are interested here in the effect of the characteristics of the tail of the distribution to long-distance dispersal we concentrate on varying α only. For comparison, we also include results obtained with the voter's model, assuming that dispersal (immigration) only occurs from the six nearest neighbor cells. The voter's model corresponds to an extreme case of short-distance dispersal. Because all sites are occupied in the lattice, we use the number of the contiguous individuals as a measure of area, A.

The species–area relationships are shown in Fig. 17.8 for Lévy stable distributions having parameters $c = 1$ and $\alpha = 1.0$, 1.5, and 2.0, and the voter's model. When dispersal distances increase (α decreases) the species–area relationships change from having a concave shape to a convex shape on a log-log plot. For small number of individuals (small areas), communities with long-distance dispersal have higher species richness, and the species–area curves rise faster than for communities with short-distance dispersal. However, when sample area increases further, the rate of accumulation of species of communities having long-distance dispersal starts to slow down, whereas the rate of accumulation of species for short-distance dispersal communities accelerates. For extremely large areas, communities with short-distance dispersal have higher species richness than communities with long-distance dispersal (see inset in Fig. 17.8). This is the exact opposite for small spatial scales, where communities with short-distance dispersal have lower species richness than communities with long-distance dispersal. Note, however, because of periodic boundary conditions there is an artificial reduction in the total number of species at large spatial scales. Chave *et al.* (2002) explained this as follows: "as additional area is added to a subset, eventually that added area becomes closer to the starting point because the landscape wraps around. Thus, that area becomes more similar to the area already in the

sample, and fewer new species are added" (Chave *et al.*, 2002). In order to check the importance of periodic boundary conditions for species richness as a function of dispersal distances in our simulations, we also studied communities without periodic boundary conditions, but results were qualitatively similar.

Our previous studies of single species spatial patterns provide a guide to understanding the relationship between the shape of the species–area relationship and dispersal distance in terms of the degree of clustering. When dispersal distances are small (voter's model and α close to 2), species tend to form clusters and occupy a well delimited range. In this case, when we sample small areas, we find just a few species, or, in some extreme cases, even monodominance. When area increases, we may find just a few more species (because they are clustered), and consequently the species–area curves rise slowly. In contrast, for communities with long-distance dispersal (smaller α), species are less clustered and more intermixed. In this case, at small spatial scales we encounter more species than in cases when species are highly clustered because of short-distance dispersal. In the most extreme case of long-distance dispersal, cluster sizes reduce to the minimum size of one individual per species. Not surprisingly, in the latter case, when area increases, the number of species rises very quickly at first. However, when we keep increasing the area, the trend reverses. Because most or all species are well mixed and encountered in relatively small areas, the rate of accumulation of species decreases.

Scaling species abundance distributions under neutrality

In this final section, we examine the influence of dispersal on the shape of relative species-abundance distributions and, in particular, how dispersal affects the shape of species-abundance distributions as sample area increases. Bell (2000, 2001) also studied in detail the shape of species-abundance distributions under neutrality; however, Bell (2000) did not consider dispersal on space explicitly, and Bell (2001) considered the spatial location of local communities explicitly but not the spatial location of each individual in its local community. Equally, Chave *et al.* (2002) analyzed how relative abundance changes at different scales, but here we also compare species-abundance distributions obtained with different dispersal kernels at the same spatial scales.

Figure 17.9 shows species-abundance distributions (species frequencies) plotted as a function of the octaves of the number of individuals (Preston curves) for different spatial scales and for $\alpha = 1.0$, plot (a), and for $\alpha = 2.0$, plot (b). In both cases the distributions have a similar pattern of change when area increases. For the smallest number of individuals the curves resemble those of a log series, with the maximum occurring for the lowest abundance class, and then monotonically decreasing. When area increases, the curves develop a maximum (mode) in intermediate abundance classes. This is reminiscent of the "unveiling" effect of the distribution first discussed by Preston (1948) (Hubbell, 2001, chapter 2). Finally, at

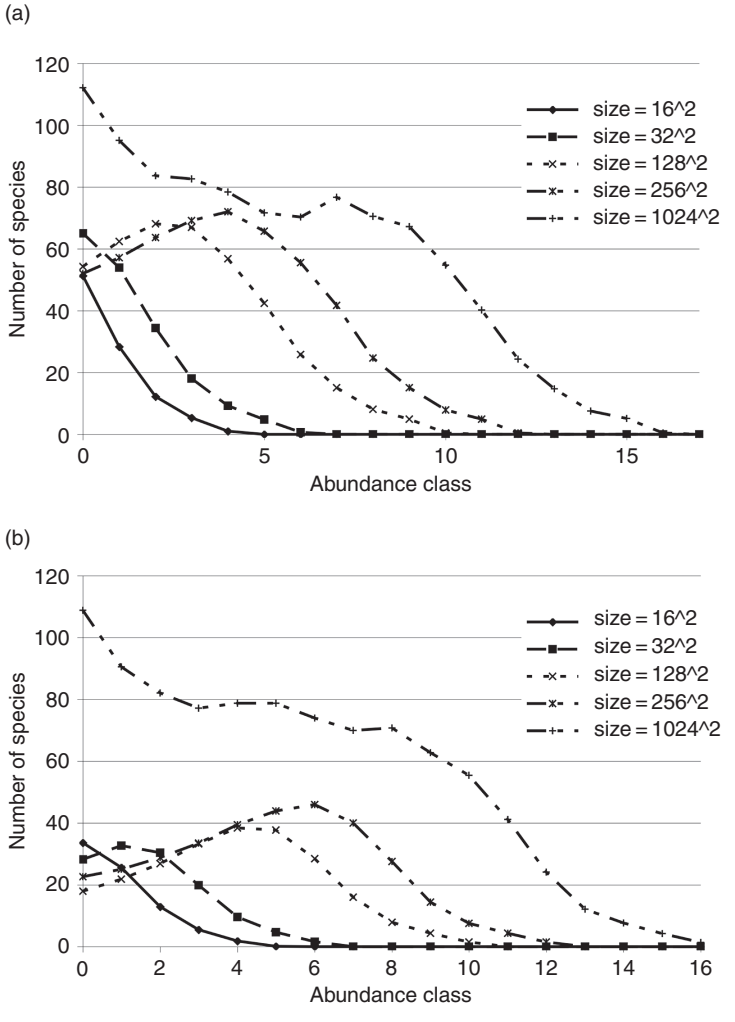

Figure 17.9 Species–abundance distributions obtained with simulations with $c = 10$, $\upsilon = 10^{-4}$, and $\alpha = 1.0$ (a) and $\alpha = 2.0$ (b) for different number of individuals: 16^2, 32^2, 128^2, 256^2, and 1024^2. The first abundance class corresponds to 1 individual, the second to 2 individuals, the third to 3–4 individuals, the fourth to 5–8, and so on, with the top value corresponding to a power of 2.

the largest scales the maximum tends to occur once again at the lowest abundance class, and the curves become more similar to a log series. Although both families of curves show the same changes as area increases, closer inspection reveals that there are quantitative differences between the curves. For small areas, the community obtained with longer dispersal distances ($\alpha = 1.0$) has more singleton species but fewer species in the higher abundance classes. This result is in agreement with the findings of the previous section because under long-distance dispersal species are more intermingled; therefore, for small areas we find, on average, fewer individuals per species. When area increases, the maximum for intermediate abundance classes first appears in the community with shorter dispersal distances. Again, this result is a consequence of the lower number of rare species at small spatial scales when dispersal distances are short because

species tend to occur in clusters. Above a certain area, both curves show a maximum for intermediate abundances. When the sample area increases further, the curves become progressively more similar, and the maximum for intermediate abundances is less obvious and it may disappear altogether. Interestingly, for the entire area, the species-abundance distributions for short-dispersal distances have a larger number of singleton species than the curves obtained for larger dispersal distances. The important conclusion is that the shape of the species-abundance distribution is not only a function of dispersal, but also a function of size of the sample area (see also Hubbell & Borda-de-Água, 2004).

Discussion and conclusions

Here we have developed a neutral model that considers space explicitly and studied the effect of long- and short-distance dispersal, first, on the spatial patterns of individual species distributions and, second, on the macroecological patterns of species–area curves and species-abundance distributions. We used Lévy stable distributions to model the dispersal kernels because their power law ("fat") tails better capture long-distance dispersal events. We used multifractals to analyze the spatial distributions obtained with simulations and compared the results with the multifractal analyses of the spatial distribution of individual tree species in BCI.

Our work on the multifractal characteristics of individual species, spatial distributions is meant as a starting point. One current problem is the general inadequacy of data sets on the large-scale distribution of species. The proper study of multifractality (or fractality) requires data sets from where we can extract scaling regions that span several orders of magnitude. Data of this sort are rare in ecology. Both our simulations (because of limiting computer time and space) and the BCI data set are no exceptions to this general problem of inadequate data sets. Given these limitations, we used the most robust method we could to obtain the multifractal spectra, the fixed-mass method, and attempted to estimate the multifractal spectrum only for those species with large sample sizes, more than 500 individuals, and for species in which we observed a scaling region for at least one order of magnitude.

Given these caveats, we arrive at three important conclusions from our multifractal analyses. The first conclusion is that a large number of species, about 90% of the species in the BCI 50 ha plot with more than 500 individuals, were well described by a multifractal pattern. The second conclusion is that the distributions obtained from the neutral theory with Lévy stable dispersal were also well described by a multifractal pattern. Third, differences among BCI species in dispersal mode and in life history were significantly correlated with differences in their multifractal spectra.

Moreover, these multifractal patterns were present in the simulations regardless of the particular parameter values of the Lévy stable distribution used to model dispersal. However, the characteristics of the multifractal spectra depended

on the value of the characteristic exponent, α, of the Lévy stable distributions. When dispersal distance decreases (large α), the spatial distributions are more heterogeneous, which is revealed in the increase of the width of the multifractal spectra, D_q. This observation raises the question of whether there is a quantitative relationship between the parameter α of the Lévy stable distributions and values of the multifractal spectrum, such as the fractal dimensions. In our limited explorations of this question, we did not find such a relationship. One reason is that there was some variability in the resulting multifractal spectra even for the same α value. A complicating issue is that not all species had the same number of individuals, which is likely to affect the estimation of the multifractal spectrum. Nevertheless, we did demonstrate a significant trend towards less clustering when dispersal distances increase, as revealed by an increase in the correlation dimension D_2, and the tendency of the multifractal spectrum to become narrower. This result was helpful in understanding the shape of the species–area curves and species-abundance distributions obtained with simulations. It has been suggested (e.g. Rosenzweig, 1995; Hubbell, 2001) that species–area relationships are triphasic. When plotted in a log-log plot they are convex near the origin, almost log-log linear on intermediate scales, i.e. scales on which they are well described by power laws, and then for very large areas they approach a slope close to 1. A slope close to 1 is usually interpreted as the result of exceeding the correlation length by sampling across regions having independent evolutionary histories and biotas. In the voter's model, a limiting slope of unity can be proven analytically (Bramson, Cox & Durrett, 1996), and Allen and White (2003) showed that a slope equal to 1 can be obtained under the assumption of restricted species ranges.

In our simulations we did not observe slopes approaching unity for large areas, but this is probably a result of the small size of the simulation lattice, and the use of periodic boundary conditions, which tend to reduce the rate of accumulation for very large areas, as mentioned. By contrast, for small and intermediate areas, we obtained curves that reproduce the shapes of those observed in real data. For intermediate scales, the species–area relationships were nearly linear in log-log plots. Note also that our simulations used the same dispersal kernel for all species, following the symmetry assumption of the neutral model. However, we know that species have different dispersal abilities. We have not yet studied what happens in this case, but the species–area relationships obtained with species having a variety of dispersal kernels may differ from the ones obtained with our simulations. We speculate that their shapes will be a mixture of the curves we obtained with the simulations and will be well described by power laws.

The region of the log-log species–area relationship in which the effect of dispersal is more visible is at small spatial scales. When dispersal distances increase, the shape of the log-log species–area relationship changes to

accelerating curves at short distances and decelerating curves at long distances. The latter is the pattern most often observed in real data sets (e.g. Condit *et al.*, 1996). However, accelerating (upward bent) curves can also be observed, as shown by Palmer (this volume) for the mountainous plants in North America. Short-distance dispersal may be one explanation for such patterns, since it is easy to imagine that mountains act as barriers to plant dispersal at a variety of spatial scales. Of course, other processes, such as habitat heterogeneity and habitat specialization, may be at work as well.

An important result, in agreement with Hubbell (2001), is that short-distance dispersal may lead to lower species richness in local communities at small scales, but to greater species richness in communities at large scales (Fig. 17.8). This means that increasing dispersal distances increases local community species richness (alpha diversity) at small scales but has a complex effect on beta diversity, first increasing and then decreasing species turnover as area increases.

Concerning species abundance distributions when plotted as Preston curves, two important results were shown with the simulations. First, and in accordance with Hubbell (2001), Chave *et al.* (2002) and Hubbell and Borda-de-Água (2004), the shape of the species–abundance distribution is a function of the sampling area, and, second, for the same sampling area, the shape of the species-abundance distribution is a function of the dispersal rate. The second result is important because it shows that comparison of the evolution of the species-abundance distributions with area for two different communities may reveal the characteristic dispersal distances of their species. In conclusion, our study emphasizes the importance of defining the sampling area relative to the spatial scale of dispersal for understanding the scaling of species-abundance distributions. One caveat to our conclusions is that all of our simulations employed the "point-mutation" mode of speciation, which generates many short-lived rare species. It is known that other models of speciation, such as "random-fission" speciation (Hubbell, 2001) or "peripheral isolate" speciation (Hubbell & Lake, 2003; Hubbell, 2005), produce different steady-state distributions of relative species abundance, with fewer rare species. In particular, changing the mode of speciation may affect our conclusions regarding the shape of the relative abundance distributions, especially the relative abundance of singleton species.

It is also important to notice that there is no distinction between local communities and metacommunity in our model as there was in Hubbell (2001). Nevertheless, our results agree with the qualitative conclusions reached by Hubbell (2001). In our case, a subset of the simulation lattice is equivalent to a local community, and a reduction in the dispersal distance is equivalent to a reduction in the immigration rate, the parameter that coupled the local communities with the metacommunity in Hubbell's original model.

The results of our simulations are also in good qualitative agreement with the observations from real data sets – in particular those from tropical forest tree communities. These results of course do not prove that tropical tree communities are neutral-symmetric. However, they do suggest that symmetric neutral theory is a good first approximation, especially with the improved dispersal model and the explicit treatment of space. These results are encouraging and mean that it is profitable to ask to what extent community-level patterns are the result of species similarities rather than to their differences. The improved theory also allows us to study the spatial distribution of individual species in far greater detail. Future work will include breaking symmetry in a variety of ways, and asking to what extent species differences must be incorporated in order to explain particular aspects of biodiversity scaling relationships in different ecological communities.

Appendix 17.I Multifractals

This appendix describes in more detail methods to characterize multifractals.

Characterization of multifractals by the box-counting method

The characterization of a multifractal requires a set of numbers, some of which correspond to fractal dimensions. Hereafter we focus exclusively on describing point distributions in a plane. There are at least three methods for obtaining these numeric descriptors for point distributions: the box-counting method, familiar to many readers, the fixed-radius method and the fixed-mass method. When describing multifractals, the box-counting method is useful mainly for heuristic reasons, but is rarely used in practical situations. Consider, for example, the distributions in Fig. 17.3. Suppose we are just interested in presence–absence, i.e. the box-counting fractal dimension. In this case, we cover the points with "boxes" (squares) and count how many boxes contain at least one point. Then we repeat this process for boxes of different sizes. The theoretical definition of fractal dimension is given by

$$D = \lim_{\varepsilon \to 0} -\frac{\log(N(\varepsilon))}{\log(\varepsilon)}, \tag{17.5}$$

where $N(\varepsilon)$ is the number of occupied boxes of linear size (side length) ε. However, in actual situations, we estimate D by plotting $\log N(\varepsilon)$ versus $\log(\varepsilon)$, and then identify a region of variation in ε over which the relationship is well approximated by a straight line (this requirement should occasionally be relaxed, as explained in Box 17.1). The slope of this line segment is equal to $-D$.

In the case of multifractals, however, we also need to take into account the proportion of points, p_i, in each box. Now the characterization of the multifractal is done in terms of a set of generalized "dimensions", D_q, obtained from the equation

$$D_q = \lim_{\varepsilon \to o} \frac{1}{q-1} \frac{\log\left(\sum_{i=1}^{N(\varepsilon)} p_i^q\right)}{\log(\varepsilon)}, \tag{17.6}$$

where q is a real number ranging from $-\infty$ to $+\infty$; to avoid the division by zero, we take the limit when q tends to 1, and the resulting formula is

$$D_1 = \lim_{\varepsilon \to o} \frac{\sum_{i=1}^{N(\varepsilon)} p_i \log(p_i)}{\log(\varepsilon)}. \tag{17.7}$$

Note that Eq. (17.5) is just a special case of Eq. (17.6) when $q = 0$, and that changing q is similar to obtaining the moments of the distribution of the p_i. The set of values of D_q is called the "D_q spectrum" of generalized "dimensions". In real world situations, in analogy with estimating the fractal dimension, we estimate D_q by looking for straight line segments in the plots of $\log\left(\sum_{i=1}^{N(\varepsilon)} p_i^q\right)$ versus $\log(\varepsilon)$. The D_q spectrum is a monotonically decreasing function of q and looks like a stretched Z (see Fig. 17.4).

The utility of obtaining the D_q spectrum by changing q is that it reveals many different and subtle attributes of a pattern of points on a plane. For example, when q is a large positive number, the sum in Eq. (17.6) is most sensitive to the largest p_i values, that is, to regions of high abundance. Conversely, when q is a small negative number, but large in absolute value, the sum in Eq. (17.6) is most sensitive to the smallest p_i values, that is, to regions of low abundance. The width of the D_q spectrum is a measure of the heterogeneity of the multifractal. Thus, for a Poisson process with no heterogeneity (complete spatial randomness) all dimensions are equal and the D_q spectrum is a straight line parallel to the q-axis.

Characterization of multifractals by the fixed-radius and fixed-mass methods

Although easy to implement, the box-counting method has problems in real applications (see Cutler, 1993). For very large boxes, all boxes are likely to be occupied, and the number of boxes increases with the Euclidean dimension of the space (2, for points in the plane). For very small boxes, all boxes contain only one point, and the number of boxes remains constant. In order to overcome these problems, some authors (e.g. Grassberger & Procaccia, 1983; Badii & Broggi, 1988) have developed alternative methods based on the distance between points (for an example of a practical application see Hirabayashi, Ito & Yoshii, 1992). These methods are based on the following relationship:

$$\langle (p_i / R^{D_q})^{q-1} \rangle \sim \text{constant}, \tag{17.8}$$

where now $p_i = m/(M-1)$, m is the number of points within radius R of a given point, i, M is the total number of points, and $< >$ denotes the average taken over all points. Based on Eq. (17.8), one can pursue two strategies to obtain D_q: the fixed-radius and the fixed-mass methods.

In the fixed-radius approach we determine how many points, m, lie within radius R of a given point i, and estimate the dependency of $p_i(R)$ on R according to

$$\langle p_i(R)^{q-1} \rangle \sim R^{\tau_q}, \tag{17.9}$$

where $\tau_q = (q-1)D_q$. For $q = 2$ we obtain an expression known as the "correlation sum"; hence the procedure used in calculating D_2 is equivalent to that for calculating Ripley's function (e.g. Diggle, 1983).

In the fixed-mass approach, we instead calculate the minimum radius from a point i, R_i, that contains m points, and we write the functional dependency $R_i(m)$ on m as

$$\langle R_i(m)^{-\tau_q} \rangle^{1/\tau_q} \sim m^{-1/D_q}. \tag{17.10}$$

Although the fixed-radius method is easier to implement than the fixed-mass method, it has the disadvantage of leading to very small scaling regions for $q < 1$, and, hence, it is not recommended for estimating D_q for $q < 1$ (Grassberger, Badii & Politi, 1988). For this reason, we recommend the use of the fixed-mass method to obtain multifractal spectra.

The steps to determine the multifractal spectra using the fixed-mass method are: (1) for every point in the set determine the minimum value of R that contains a specified number of points, m; (2) repeat the previous step for different values of m; (3) choose different values of τ_q and check if $\log(\langle R_i(m)^{-\tau_q} \rangle^{1/\tau_q})$ as a function of $\log(m)$ can be appropriately described by a linear relationship for some scaling region (but see Box 17.1); (4) if a scaling region is found, estimate the slope ($= -1/D_q$); and (5) once D_q is known, determine q from $q = 1 + \tau_q/D_q$.

An important difference between the fixed-radius and the fixed-mass method is that in the former we vary q, while in the latter we vary τ. This implies that in the fixed-mass method we do not have control over the obtained values of q. In some cases, however, we may like to know the exact value of a given D_q (D_2, for example). One solution is to choose several values of τ within the range of values that we predict to lead to $q = 2$, and choose the obtained value of q that is closest to 2.

In most practical situations, it is also desirable to introduce corrections for boundaries. We suggest the correction method used in the statistical analysis of spatial point processes together with Ripley's function (see Diggle, 1983).

Acknowledgments

LBA thanks the kind hospitality provided by the Pacific Forestry Centre, Victoria BC, Canada. We thank Jayanth Banavar, Amos Maritan, and Igor Volkov for stimulating discussions. We thank David Storch, Pablo Marquet, and Jérôme

Chave for suggestions that considerably improve the content and presentation of this chapter. This work was partially carried out under a postdoctoral fellowship from Simon Fraser University and a grant from the National Science Foundation (DEB 0346488).

References

Allen, A. P. & White, E. P. (2003). Effects of range size on species-area relationships. *Evolutionary Ecology Research*, **5**, 493–499.

Badii, R. & Broggi, G. (1988). Measurement of the dimension spectrum $f(\alpha)$: fixed mass approach. *Physics Letters A*, **131**, 339–343.

Badii, R. & Politi, A. (1984). Intrinsic oscillations in measuring the fractal dimension. *Physics Letters A*, **104**, 303–305.

Bell, G. (2000). The distribution of abundance in neutral communities. *American Naturalist*, **155**, 606–617.

Bell, G. (2001). Neutral macroecology. *Science*, **293**, 2413–2418.

Bramson, M., Cox, J. T. & Durrett, R. (1996). Spatial models for species-area curves. *Annals of Probability*, **24**, 1721–1751.

Chambers, J. M., Mallows, C. L. & Stuck, B. W. (1976). A method for simulating stable random variables. *Journal of the American Statistical Association*, **71**, 340–344.

Chave, J. & Leigh Jr., E. G. (2002). A spatially explicit neutral model of β-diversity in tropical forests. *Theoretical Population Biology*, **62**, 153–168.

Chave, J., Muller-Landau, H. C. & Levin, S. A. (2002). Comparing classical community models: theoretical consequences for patters of diversity. *American Naturalist*, **159**, 1–23.

Clark, J. S., Fastie, C., Hurtt, G., *et al.* (1998). Reid's paradox of rapid plant migration. *Bioscience*, **48**, 13–24.

Clark, J. S., Silman, M., Kern, R., Macklin, E. & HilleRisLambers, J. (1999). Seed dispersal near and far: patterns across temperate and tropical forests. *Ecology*, **80**, 1475–1494.

Condit, R., Hubbell, S. P., LaFrankie, J. V., *et al.* (1996). Species-area and species-individual relationships for tropical trees: a comparison of three 50 ha plots. *Journal of Ecology*, **84**, 549–562.

Cutler, C. D. (1993). A review of the theory and estimation of fractal dimension. In *Dimension Estimation and Models*, ed. H. Tong, pp. 1–107. Singapore: World Scientific.

Diggle, P. J. (1983). *Statistical Analysis of Spatial Point Processes*. London: Academic Press.

Durrett, R. & Levin, S. (1996). Spatial models for species-area curves. *Journal of Theoretical Biology*, **179**, 119–127.

Etienne, R. S. & Olff, H. (2004). A novel genealogical approach to neutral biodiversity theory. *Ecology Letters*, **7**, 170–175.

Evertsz, C. J. G. & Mandelbrot, B. B. (1992). Multifractal measures. In *Chaos and Fractals. New Frontiers of Science*, ed. H. O. Peitgen, H. Jürgens & D. Saupe, pp. 921–953. New York: Springer-Verlag.

Gnedenko, B. V. & Kolmogorov, A. N. (1954). *Limit Distributions for Sums of Independent Random Variables*. Cambridge, MA: Addison-Wesley.

Grassberger, P. & Procaccia I. (1983). Characterization of strange attractors. *Physical Review Letters*, **50**, 346–349.

Grassberger, P., Badii, R. & Politi, A. (1988). Scaling laws for invariant measures on hyperbolic and nonhyperbolic atractors. *Journal of Statistical Physics*, **51**, 135–178.

Halley, J. M. & Iwasa, Y. (1998). Extinction rate of a population under both demographic and environmental stochasticity. *Theoretical Population Biology*, **53**, 1–15.

Hirabayashi, T., Ito, K. & Yoshii, T. (1992). Multifractal analysis of earthquakes. *Pure and Applied Geophysics*, **138**, 591–610.

Holley, R. A. & Liggett, T. M. (1975). Ergodic theorems for weakly interacting systems and the voter model. *Annals of Probability*, **3**, 643–663.

Houchmandzadeh, B. & Vallade, M. (2003). Clustering in neutral ecology. *Physical Review E*, **68**, Art. No. 061912.

Hubbell, S. P. (1997). A unified theory of biogeography and relative species abundance and its applications to tropical rain forests and coral reefs. *Coral Reefs*, **16** (suppl.), S9–S21.

Hubbell, S. P. (2001). *The Unified Neutral Theory of Biodiversity and Biogeography*. Princeton: Princeton University Press.

Hubbell, S. P. (2005). Neutral theory of biodiversity and biogeography and Stephen Jay Gould. *Paleobiology*, **31** (suppl.), 122–132.

Hubbell, S. P. & Borda-de-Água L. (2004). The distribution of relative species abundance in local communities under neutrality: a response to the comment by Chisholm & Burgman. *Ecology*, **85**, 3175–3178.

Hubbell, S. P. & Foster, R. B. (1983). Diversity of canopy trees in a neotropical forest and implications for the conservation of tropical trees. In *Tropical Rain Forest: Ecology and Management*, ed. S. J. Sutton, T. C. Whitmore & A. C. Chadwick, pp. 25–41. Oxford: Blackwell.

Hubbell, S. P. & Lake, J. K. (2003). The neutral theory of biodiversity and biogeography, and beyond. In *Macroecology: Concepts and Consequences*, ed. T. M. Blackburn & K. J. Gaston, pp. 45–63. Oxford: Blackwell Science.

Jones, F. A., Chen, J., Weng, G. J. & Hubbell, S. P. (2005). A genetic evaluation of seed dispersal in a Neotropical tree, *Jacaranda copaia* (Bignoniaceae). *American Naturalist*, **166**, 543–555.

Kot, M., Lewis, M. A. & Van den Driessche, P. (1996). Dispersal data and the spread of invading organisms. *Ecology*, **77**, 2027–2042.

Lewis, M. A. (1997). Variability, patchiness, and jump dispersal in the spread of an invading population. In *Spatial Ecology: The Role of Space in Population Dynamics and Interspecific Interactions*, ed. D. Tilman & P. Kareiva, pp. 46–74. Princeton: Princeton University Press.

Liebovitch, L. S. (1998). *Fractals and Chaos Simplified for the Life Sciences*. Oxford: Oxford University Press.

MacArthur, R. H. & Wilson, E. O. (1967). *The Theory of Island Biogeography*, Princeton: Princeton University Press.

Mandelbrot, B. B. (1977). *Fractals: Form, Chance, and Dimension*. San Francisco: W. H. Freeman.

Mandelbrot, B. B. (1997). *Fractals and Scaling in Finance: Discontinuity, Concentration, Risk*. New York: Springer.

Manly (1997). *Randomization, Bootstrap and Monte Carlo Methods in Biology*. 2nd edn. London: Chapman & Hall/CRC.

Mantegna, R. N. & Stanley, H. E. (2000). *An Introduction to Econophysics: Correlations and Complexity in Finance*. Cambridge: Cambridge University Press.

McKane, A. J, Alonso, D. & Solé, R. V. (2004). Analytic solution of Hubbell's model of local community dynamics. *Theoretical Population Biology*, **65**, 67–73.

Meneveau, C. & Sreenivasan, K. R. (1989). Measurements of $f(\alpha)$ from scaling histograms and applications to dynamical systems and fully developed turbulence. *Physics Letters A*, **137**, 103–112.

Muller-Landau, M. C., Dalling, J. W., Harms, K. E., *et al*. (2004). Seed dispersal and density-dependent seed and seedling survival in *Trichilia turbeculata* and *Miconia argentea*. In *Tropical Forest Diversity and Dynamism: Findings From a Large-scale Plot Network*, ed. C. Losos & E. G. Leigh, Jr., pp. 340–362. Chicago: University of Chicago Press.

Nagylaki, T. (1974). The decay of genetic variability in geographically structured populations. *Proceedings of the National Academy of Sciences of the USA*, **71**, 2932–2936.

Nathan, R. & Muller-Landau, H. (2000). Spatial patterns of seed dispersal, their determinants and consequences for recruitment. *Trends in Ecology and Evolution*, **15**, 278–285.

Petit, J. R., Pineau, E., Demesure, B., Bacilieri, R., Ducousso, A. & Kremer, A. (1997). *Proceedings of the National Academy of Sciences of the USA*, **94**, 9996–10001.

Preston, F. W. (1948). The commonness, and rarity, of species. *Ecology*, **29**, 254–283.

Rosenzweig, M. L. (1995). *Species Diversity in Space and Time*. Cambridge: Cambridge University Press.

Silvertown, J., Holtier, J. S., Johnson, J. & Dale, P. (1992). Cellular automaton models of interspecific competition for space – the effect of pattern on process. *Journal of Ecology*, **80**, 527–534.

Vallade, M. & Houchmandzadeh, B. (2003). Analytical solution of a neutral model of biodiversity. *Physical Review E*, **68**, Art. No. 061902.

Volkov, I., Banavar, J. R., Hubbell, S. P. & Maritan, A. (2003). Neutral theory and relative species abundance in ecology. *Nature*, **424**, 1035–1037.

Volkov, I., Banavar, J., He, F., Hubbell, S. P. & Maritan, A. (2005). Density dependence explains tree species abundance and diversity in tropical forests. *Nature*, **438**, 658–661.

Weiss, G. H. (1994). A primer of random walkology. In *Fractals in Science*, ed. A. Bunde & S. Havlin, pp. 119–161. Berlin: Springer-Verlag.

West B. J. & Deering, W. (1994). Fractal physiology for physicists: Lévy statistics. *Physics Reports*, **246**, 1–100.